

# Interlayer Hydrogen-Bonded Covalent Organic Frameworks as High-Performance Supercapacitors

Arjun Halder,<sup>a,b</sup> Meena Ghosh,<sup>a,b</sup> Abdul Khayum M,<sup>a,b</sup> Saibal Bera,<sup>a,b</sup> Matthew Addicoat,<sup>d</sup> Himadri Sekhar Sasmal,<sup>c</sup> Suvendu Karak,<sup>a,b</sup> Sreekumar Kurungot<sup>a,b</sup> and Rahul Banerjee<sup>\*c</sup>

<sup>a</sup>Academy of Scientific and Innovative Research (AcSIR), CSIR-National Chemical Laboratory, Dr. Homi Bhabha Road, Pune-411008, India.

<sup>b</sup>Physical/Materials Chemistry Division, CSIR-National Chemical Laboratory, Dr. Homi Bhabha Road, Pune-411008, India.

<sup>c</sup>Department of Chemical Sciences, Indian Institute of Science Education and Research (IISER) Kolkata, Mohanpur Campus, Mohanpur, 741246, India.

<sup>d</sup>School of Science and Technology, Nottingham Trent University, Clifton Lane, NG11 8NS Nottingham, United Kingdom.

## Supporting Information Placeholder

**ABSTRACT:** Covalent organic frameworks (COFs) have emerged as promising electrode materials in supercapacitors (SCs). However, their insoluble powder like nature, poor capacitive performance in pristine form, integrated with inferior electrochemical stability is a primary concern for their long-term use in electrochemical-devices. Keeping this in perspective, herein, we report a redox active and hydrogen bonded COF with ultrahigh stability in conc. H<sub>2</sub>SO<sub>4</sub> (18 M), conc. HCl (12 M) and NaOH (9 M). The as-synthesized COF fabricated as thin sheets were efficiently employed as a free-standing supercapacitor electrode material using 3 M aq. H<sub>2</sub>SO<sub>4</sub> as an electrolyte. Moreover, the pristine COF sheet showcased outstanding areal capacitance 1600 mFcm<sup>-2</sup> (gravimetric 169 Fg<sup>-1</sup>) and excellent cyclic stability (> 1,00,000) without compromising its capacitive performance or coulombic efficiency. Moreover, as a proof-of-concept, a solid-state supercapacitor device was also assembled and subsequently tested.

Covalent organic frameworks (COFs) have attracted enormous scientific attention because of their tunable porosity and periodically ordered structures with high atomic precision.<sup>1</sup> Recently, COFs have been identified as promising materials for supercapacitors (SCs), owing to their long-range ordered arrangement with high accessible surface area which is ideal for efficient ion transport within the electrode-electrolyte interface.<sup>2</sup> Also, advantages of reticular structural construction led to the explicit incorporation of redox-active functionalities within the porous COF backbone thereby resulting in them becoming suitable for pseudo-capacitive energy storage.<sup>3</sup> However, their insoluble granular nature (hence the difficulty in the electrode fabrication), inferior capacitive performance in pristine form due to their non-conductive nature and poor electrochemical stability restrict their potential usage in SCs. Therefore, the fabrication of a COF based high performance electrode material, with sizeable electrolyte-accessible surface areas integrated with excellent cyclic stability in mordant electrolyte condition is still challenging and highly desirable.

The  $\beta$ -keto-enamine-based COFs, since their discovery, have

enriched the COF literature as promising pseudo-capacitors.<sup>4</sup> However, their usage mostly in powdered form (or in few cases on the support), low capacitive performance in the pure state as well as limited cyclic stability compared to EDLCs (electrical double layer capacitors)<sup>5</sup> during the electro-chemical process have conveyed a restriction towards their extensive usage. Additionally, the non-conjugative nature of  $\beta$ -keto-enamine COFs could make them sluggish towards good electrochemical response compared to more conjugated imine (C=N) based COFs. Although, additional conductive additives or post functionalization could enhance the capacitive performance, they would lead to further synthetic hurdles, and their presence could dramatically affect the active surface area due to the extensive pore blockage.<sup>6</sup>

Keeping this in perspective, herein we report an imine-based, redox active COF **TpOMe-DAQ** that has been constructed from 2,4,6-trimethoxy-1,3,5-benzenetricarbaldehyde (TpOMe) and 2,6-diaminoanthraquinone (DAQ) as building units. The judicious choice of such linker units could combine both electrochemical stability (due to the explicit incorporation of the methoxy functionality) and reversible redox response due to the quinone/hydroquinone transformation (DAQ amine) for energy storage.<sup>4b, 7</sup> **TpOMe-DAQ** exhibits ultrahigh chemical stability in drastic conditions [strong acids (18 M H<sub>2</sub>SO<sub>4</sub>; 12 M HCl) or bases (9 M NaOH)] due to the presence of interlayer C-H $\cdots$ N H-bonding [ $D=3.26$  Å,  $d= 2.17$  Å,  $\theta=168.2^\circ$ ;  $D= 3.16$ ,  $d=2.07$ ,  $\theta=165.8^\circ$ ] between methoxy C-H and the imine 'N' atom of adjacent layers.<sup>8</sup> Furthermore, this COF could be fabricated as uniform and continuous thin sheets even in centimeter scale while maintaining the thickness of  $\sim 200$   $\mu\text{m}$  (**Figure 1a-d**, **Figure S1**). These findings encouraged us to utilize these COF thin sheets as free-standing supercapacitor electrodes using concentrated aq. H<sub>2</sub>SO<sub>4</sub> (2 and 3 M) as an electrolyte. Moreover, in three electrode assemblies using 3 M aq. H<sub>2</sub>SO<sub>4</sub>, the COF thin sheets showcased exceptionally high areal capacitance of 1600 mFcm<sup>-2</sup> (gravimetric 169 Fg<sup>-1</sup>) which is the highest value ever achieved in pure COF based SCs and also comparable to other promising electrode materials (**Tables S1, S2**). **TpOMe-DAQ**, in 2 M aq. H<sub>2</sub>SO<sub>4</sub> showcased outstanding capacitive performance (1280 mFcm<sup>-2</sup> and 135 Fg<sup>-1</sup>) and galvanostatic charge-discharge (GCD) cyclic stability exceeding 1,00,000 cycles without compromising the capacitance.

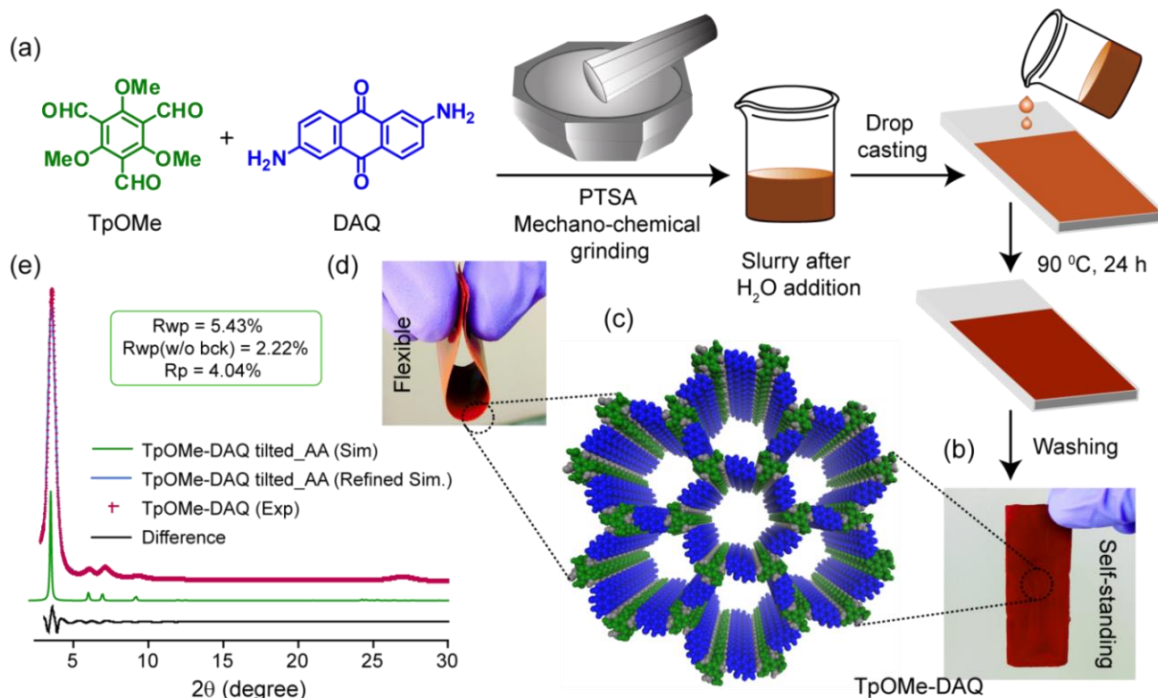


**Figure 1.** (a) General synthetic scheme of the **TpOME-DAQ** thin sheet from aldehyde (**TpOME**) and amine **DAQ** by PTSA (*p*-toluenesulfonic acid) mediated mechano-chemical grinding approach. (b and d) Digital images show the self-standing and flexible nature of the thin sheet. (c) Tilted\_AA model of **TpOME-DAQ**. (e) Comparison among the experimental (red) with simulated eclipsed tilted-AA (green), refined simulated (blue) PXRD patterns and Pawley refinement difference (black) for **TpOME-DAQ** COF.

Additionally, in a solid-state device, the COF thin sheet could retain ~65% of its initial capacitance even after 50,000 continuous charge-discharge cycles, keeping the coulombic efficiency intact.

The formation of **TpOME-DAQ** was confirmed by the PXRD analysis. The PXRD pattern shows five distinct characteristic peaks at 3.5, 6.0, 7.1, 9.3 and 27.1 ( $\pm 0.1$ ,  $2\theta$ ) which belongs to the reflections from the planes 100, 110, 200, 210 and 001 respectively. The experimental PXRD patterns fit with the simulated tilted-AA structure [Rwp-5.4%, Rwp (w/o bck)- 2.2% and Rp-4.1%] (**Figure 1e**, **S2**). Moreover, Pawley refinement was taken into consideration to analyze the unit cell parameters (Space group *P1*;  $a=29.8$ ,  $b=29.8$ ,  $c=3.7$  &  $\alpha=87.0$ ,  $\beta=83.2$ ,  $\gamma=59.1^\circ$  for tilted-AA) (**Figure S3**, **Table S3**). The FTIR analysis of the **TpOME-DAQ** revealed the complete disappearance of the N–H stretching ( $3420\text{--}3199\text{ cm}^{-1}$ ) of the **DAQ** amine and C=O stretching at  $1682\text{ cm}^{-1}$  from **TpOME** aldehyde (**Figure S4**). The newly formed C=N stretching appeared at  $1621\text{ cm}^{-1}$  whereas the C=O stretching ( $1660\text{ cm}^{-1}$  in **DAQ** amine) was observed at  $1673\text{ cm}^{-1}$ . The solid-state  $^{13}\text{C}$  CP-MAS spectra showed the C=O chemical shift at 180.8 ppm belonging to the **DAQ** (quinone C=O) whereas for C=N it appeared at 147.7 ppm. The signatures of aromatic and methoxy ( $-\text{OCH}_3$ ) carbons appeared at 153-108 and 64 ppm respectively (**Figure S5**).

The porosity/effective surface area of an electrode material plays a very crucial role in designing electrodes for EDLCs or pseudo-capacitive energy storage materials because it reveals the electrode's ability to hold electrolytes/ions.<sup>5</sup> Notably, the **TpOME-DAQ** COF achieved the highest BET surface area of  $1734\text{ m}^2\text{g}^{-1}$  (average  $1531\text{ m}^2\text{g}^{-1}$ ) with pore diameter estimated as 2.3 nm reflecting its meso-porous nature (**Figure S6**). Thermogravimetric analysis (TGA;  $\text{N}_2$  atmosphere) revealed framework stability up to  $300^\circ\text{C}$  (**Figure S7**). **TpOME-DAQ** was treated in different solvents (protic or aprotic) and in other drastic conditions where the material could retain its PXRD pattern and FTIR spectra concerning the pristine COF hence signifying its chemical

robustness (**Figures 2c**, **S8-S10**). The BET surface area of the material was evaluated as 1520, 1486, 1479,  $1107\text{ m}^2\text{g}^{-1}$  compared to the as-synthesized ( $1531\text{ m}^2\text{g}^{-1}$ ) COF after treatment in conc. HCl (12 M; 7 days), dil.  $\text{H}_2\text{SO}_4$  (9 M; 7 days), conc.  $\text{H}_2\text{SO}_4$  (18 M; 3 days), and in NaOH (1 day; 9 M) respectively (**Figure S10**). The exceptionally high chemical stability was believed due to the presence of interlayer C–H $\cdots$ N H-bonding [ $D=3.26\text{ \AA}$ ,  $d=2.17\text{ \AA}$ ,  $\theta=168.2^\circ$ ;  $D=3.16$ ,  $d=2.07$ ,  $\theta=165.8^\circ$ ] which protect the imine bond from being hydrolysed in such abrasive conditions (**Figures 2b**, **S13**; **Table S4**).<sup>7</sup> The existence of interlayer C–H $\cdots$ N H-bonding in **TpOME-DAQ** was realized from similar H-bonding reported in the small molecule crystal structures and also revealing its high quality FTIR spectrum compared to non-hydrogen bonded reference monomer molecule **TpOME-Ani** (**Figure S13-S18** & **Table S4**, **S5**). The mechanical strength of **TpOME-DAQ** thin sheets was evaluated using stress-strain measurement where it revealed ~3.5% of the breaking strain (**Figure S11**).

This excellent chemical stability along with long-range ordered pore channels, judiciously functionalized with redox-active groups enabled us to employ **TpOME-DAQ** as a free-standing electrode for SCs. The free-standing thin sheets were fabricated using simple hand-casting of resulted slurry (a mixture of precursors) on a suitable glass slide (ca. area  $\sim 5 \times 2\text{ cm}^2$ ) with subsequent heating at  $90^\circ\text{C}$  for 24 h (**Figure 1 a-d**, **Figure S1**). SEM revealed that the thin sheet (thickness  $\sim 200\text{--}220\text{ }\mu\text{m}$ ) is composed of small crystallites (length ca.  $1\text{--}3\text{ }\mu\text{m}$ ) that are perfectly packed to produce the self-standing and crack-free nature (**Figures 2f**, **S12**).<sup>9</sup> Initially, in the three-electrode assembly, a COF sheet with  $2.5 \times 3.0\text{ mm}^2$  area exposed in the electrolyte was used as the working electrode and a piece of grafoil was employed as a counter electrode whereas the potential (1 V window;  $-0.50$  to  $+0.50\text{ V}$ ) was recorded with reference to the Hg/Hg<sub>2</sub>SO<sub>4</sub> electrode using aq.  $\text{H}_2\text{SO}_4$  (2 and 3 M) as an electrolyte (**Section S-7**, **Figure S19**). During cyclic voltammetry (CV) analysis, the scan rate was set from  $1\text{ mVs}^{-1}$  to a maximum of  $500\text{ mVs}^{-1}$ , where a pair of

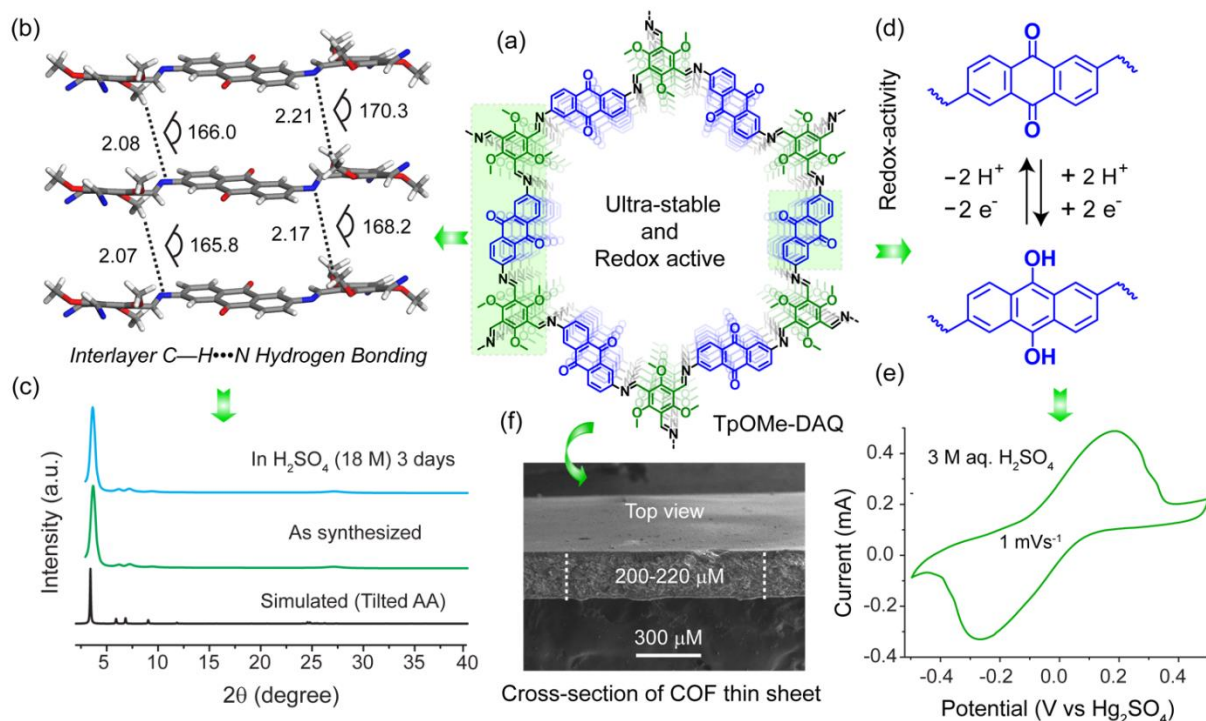


**Figure 2.** (a) Layered structure of **TpOMe-DAQ**. (b) The interlayer C–H···N H-bonding in **TpOMe-DAQ** based on distances (H to N atom; Å) shown with dotted line and angles (C–H···N) in degree (layers spaced out for clear representation). (c) PXRD of the sheet before and after treatment in H<sub>2</sub>SO<sub>4</sub> (18 M). (d) Redox behavior of **TpOMe-DAQ** through reversible quinone to hydroquinone transformation. (e) Cyclic voltammetry of the as-synthesized sheet in 3 M H<sub>2</sub>SO<sub>4</sub> using 10 mV s<sup>-1</sup> potential scanning. (f) Cross-section SEM analysis of **TpOMe-DAQ** thin sheet.

quasi-reversible redox peaks were observed at a lower scan rate of 1 mVs<sup>-1</sup> signifying the pseudo-capacitive behavior of the COF (Figures 3a, S24, S26). During the electrochemical analysis, the occurrence of the reversible Faradic reaction could be ascribed to the reversible switching between quinone (C=O) and hydroquinone (C–OH) transformation (associated to DAQ amine) (Figure 2d, 2e). The GCD analysis was performed at various current densities such as 3.3, 6.7 and 13.3 mAcm<sup>-2</sup> whereas the capacitance value was estimated from the overall discharge time (Figure 3b). During 3.3 mAcm<sup>-2</sup> scanning the areal capacitance, moved from 2 to 3 M electrolyte concentration, enhances from 1280 (135 Fg<sup>-1</sup>) to 1600 mFcm<sup>-2</sup> (169 Fg<sup>-1</sup>) which we believe is due to the availability of more H<sup>+</sup> ions around the redox-active quinone (C=O) centers (Section S-7; Figures S20, S21). Notably, for applications in flexible or wearable electronics, measurement of areal capacitance is significant to unveil effective specific capacitance of the electrode.<sup>10</sup> Moreover, considering its moderate acid strength and higher capacitance value (1280 mFcm<sup>-2</sup>) with a significant current response, 2 M electrolyte concentration was used for the remaining studies. From GCD experiments (10 mAcm<sup>-2</sup>; 1 cm<sup>2</sup> area exposed), we could observe an increment of initial capacitance running up to 30,000 cycles, which we believe could be due to the accessibility of a greater number of redox-active centers by the electrolytes, hence its activation as the cycling progressed. However, saturation occurred after that and showcased high cycle life even exceeding 1,00,000 continuous charge-discharge cycles without compromising its capacitance or coulombic efficiency (Figures 3c, S25). Furthermore, the CV and GCD comparison of the thin sheet before and after cyclic stability revealed only slight alteration in their overall curving features without leading to any alternative redox peaks while maintaining other material properties (Figure 3d, e, S22, S23). Subsequently, we could fabricate a symmetric solid-state supercapacitor device using two 1 cm<sup>2</sup> pristine COF thin sheets where we could achieve the high areal capac-

itance of 84 mFcm<sup>-2</sup> (8.8 Fg<sup>-1</sup>) with energy and power density of ~2.9 μWhcm<sup>-2</sup> and ~61.8 μWcm<sup>-2</sup> respectively using 2 M aq. H<sub>2</sub>SO<sub>4</sub>/PVA gel (polyvinyl alcohol) as an electrolyte (Figure S26). Electrochemical impedance spectroscopy (EIS) was used to calculate the electrochemical series resistance of the **TpOMe-DAQ** thin sheet (Figure S29). Notably, **TpOMe-DAQ** exhibits good cyclic stability in the device, with ~65% retention of its initial capacitance even operating over 50,000 continuous charge-discharge cycles at a current density of 5 mA cm<sup>-2</sup> (Figure S26e, S27, S28). In either case, this is the highest cyclic stability (both in two- and three-electrode assemblies) ever achieved in COF based free-standing supercapacitor studies, even when employing 2 M aq. H<sub>2</sub>SO<sub>4</sub> as an electrolyte. Moreover, as-a-proof of concept study, a 1.8 V LED was kindled for 20 sec using three solid-state devices (prepared under similar conditions) connected in a series and charged in a 3 V potential window (Figure 3f, S30, S31).

In summary, a redox-active chemically stable COF was employed as a self-standing supercapacitor electrode material. We believe that the high chemical stability is due to the effect of both steric and hydrophobic protection of imine (C=N) bonds by the neighboring –OCH<sub>3</sub> functionality and the interlayer C–H···N H-bonding. Moreover, the material exhibits an exceptionally high areal capacitance of 1600 mFcm<sup>-2</sup> whereas the energy was believed to be stored in the form of EDLC as well as pseudo-capacitive owing to its high porosity and redox transformation between quinone to hydroquinone respectively. The chemical robustness of the COF enabled us to execute the electrochemical study using extreme electrolyte concentrations (2 M aq. H<sub>2</sub>SO<sub>4</sub>/PVA gel) where it showcased a long cycle life (> 50,000) with 65% capacitance retention when operating in a solid-state device. We believe that the overall strategic design-- and fabrication of the COF thin sheets with long-standing and high performing supercapacitor electrodes, could pave its future application in electrochemical devices.

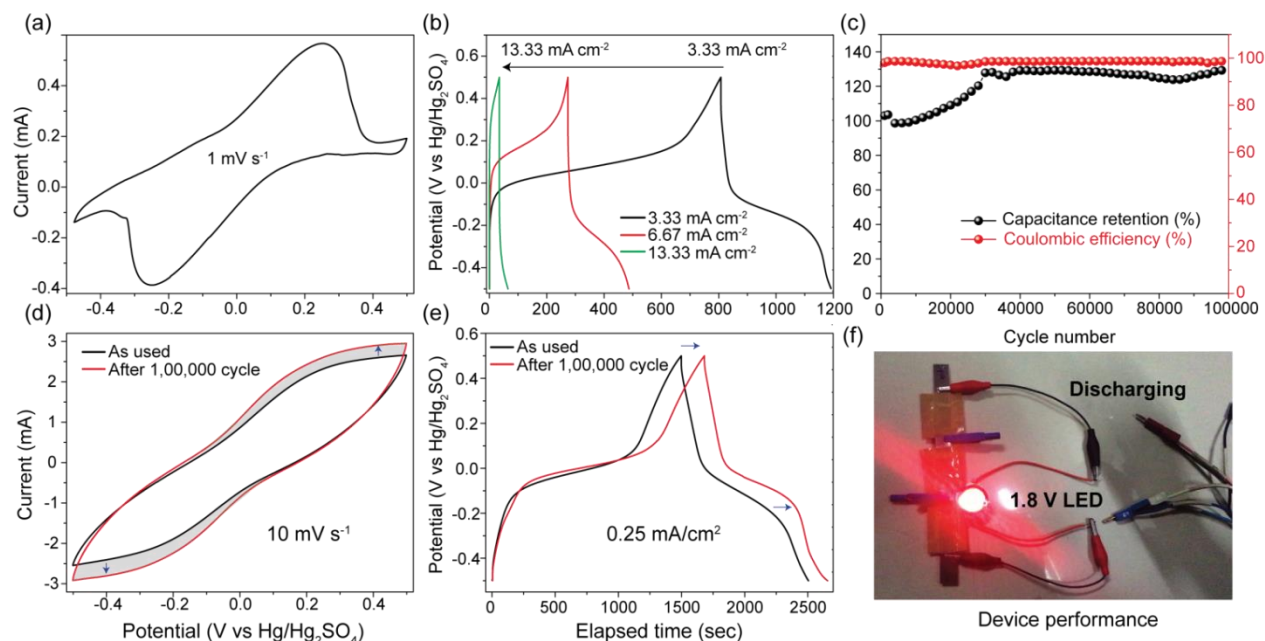


**Figure 3.** The three-electrode assembly using 2M aq.  $\text{H}_2\text{SO}_4$ - (a) CV and (b) GCD using  $7.5 \text{ mm}^2$  active area; (c) cyclic stability performance ( $10 \text{ mA cm}^{-2}$ ), (d, e) CV and GCD comparison before and after 1,00,000 cyclic performances using  $1 \text{ cm}^2$  active area; and (f) Enkindling of 1.8 V LED using three solid-state-device connected in a series using  $1 \text{ cm}^2$  active area of a **TpOMe-DAQ** thin sheets.

## ASSOCIATED CONTENT

### Supporting Information

Experimental procedures and characterization data. This material is available free of charge via the Internet at <http://pubs.acs.org>.

## AUTHOR INFORMATION

### Corresponding Author

r.banerjee@ncl.res.in

### Notes

The authors declare no competing financial interests.

## ACKNOWLEDGMENT

AH, MG, HSS and SB acknowledge CSIR, AK and SK acknowledge UGC, India. R.B. acknowledges IISER-Kolkata and the Alexander von Humboldt Foundation. MA acknowledges the Hamilton HPC facility at NTU.

## REFERENCES

- (a) Doonan, C. J.; Tranchemontagne, D. J.; Glover, T. G.; Hunt, J. R.; Yaghi, O. M. *Nat. Chem.* **2010**, *2*, 235. (b) Kuhn, P.; Antonietti, M.; Thomas, A. *Angew. Chem., Int. Ed.* **2008**, *47*, 3450. (c) Uribe-Romo, F. J.; Hunt, J. R.; Furukawa, H.; Klöck, C.; O’Keeffe, M.; Yaghi, O. M. *J. Am. Chem. Soc.* **2009**, *131*, 4570. (d) Ascherl, L.; Sick, T.; Margraf, J. T.; Lapidus, S. H.; Calik, M.; Hettstedt, C.; Karaghiosoff, K.; Döblinger, M.; Clark, T.; Chapman, K. W.; Auras, F.; Bein, T. *Nat. Chem.* **2016**, *8*, 310. (e) Sun, A.; Aguila, B.; Perman, J.; Nguyen, N.; Ma, S. *J. Am. Chem. Soc.* **2016**, *138*, 15790. (f) Han, X.; Xia, Q.; Huang, J.; Liu, Y.; Tan, C.; Cui, Y. *J. Am. Chem. Soc.* **2017**, *139*, 8693. (g) Liu, X-H.; Guan, C-Z.; Ding, S-Y.; Wang, W.; Yan, H-J.; Wang, D.; Wan, L-J. *J. Am. Chem. Soc.* **2013**, *135*, 10470. (h) Côté, A. P.; Benin, A. I.; Ockwig, N. W.; O’Keeffe, M.; Matzger, A. J.; Yaghi, O. M. *Science* **2005**, *310*, 1166. (i) El-Kaderi, H. M.; Hunt, J. R.; Mendoza-Cortés, J. L.; Côté, A. P.; Taylor, R. E.; O’Keeffe, M.; Yaghi, O. M. *Science* **2007**, *316*, 268. (j) Liu, Y.; Ma, Y.; Zhao, Y.; Sun, X.; Gándara, F.; Furukawa, H.; Liu, Z.; Zhu, H.; Zhu, C.;

Suenaga, K.; Oleynikov, P.; Alshammari, A. S.; Zhang, X.; Terasaki, O.; Yaghi, O. M. *Science* **2016**, *351*, 365.

- (a) Lanni, L. M.; Tilford, R. W.; Bharathy, M.; Lavigne, J. J. *J. Am. Chem. Soc.* **2011**, *133*, 13975. (b) Ma, Y.-X.; Li, Z.-J.; Wei, L.; Ding, S.-Y.; Zhang, Y.-B.; Wang, W. *J. Am. Chem. Soc.* **2017**, *139*, 4995. (c) ElSabbahy, M.; Wooley, K. L. *Chem. Soc. Rev.* **2012**, *41*, 2545. (d) Vyas, V.S.; Vishwakarma, M.; Moudrakovski, I.; Haase, F.; Savasci, G.; Ochsenfeld, C.; Spatz, J. P.; Lotsch, B. V. *Adv. Mater.* **2016**, *28*, 8749. (e) Wang, S.; Wang, Q.; Shao, P.; Han, Y.; Gao, X.; Ma, L.; Yuan, S.; Ma, X.; Zhou, J.; Feng, X.; Wang, B. *J. Am. Chem. Soc.* **2017**, *139*, 4258.

3. (a) Chandra, S.; Roy Chowdhury, D.; Addicoat, M.; Heine, T.; Paul, A.; Banerjee, R. *Chem. Mater.* **2017**, *29*, 2074.

- (a) Kandambeth, S.; Mallick, A.; Lukose, B.; Mane, M. V.; Heine, T.; Banerjee, R. *J. Am. Chem. Soc.* **2012**, *134*, 19524. (b) DeBlase, C. R.; Silberstein, K. E.; Truong, T.-T.; Abruña, H. D.; Dichtel, W. R. *J. Am. Chem. Soc.* **2013**, *135*, 16821. (c) DeBlase, C. R.; Hernandez-Burgos, K.; Silberstein, K. E.; Rodriguez-Calero, G. G.; Bisbey, R. P.; Abruña, H. D.; Dichtel, W. R. *ACS Nano* **2015**, *9*, 3178.

5. (a) Winter M.; Brodd, R. J. *Chem. Rev.* **2004**, *104*, 4245. (b) Simon, P.; Gogotsi, Y. *Nat. Mater.* **2008**, *7*, 845. (c) Wang, G.; Zhang, L.; Zhang, J. *Chem. Soc. Rev.* **2012**, *41*, 797. (d) Das, S.; Chakraborty, P.; Mondal, S.; Shit, A.; Nandi, A. K. *ACS Appl. Mater. Interfaces* **2016**, *8*, 28055.

6. Mulzer, C. R.; Shen, L.; Bisbey, R. P.; McKone, J. R.; Zhang, N.; Abruña, H. D.; Dichtel, W. R. *ACS Cent. Sci.* **2016**, *2*, 667. (b) Xu, F.; Xu, H. Chen, X.; Wu, D.; Wu, Y.; Liu, H.; Gu, C.; Fu, R.; Jiang, D. *Angew. Chem., Int. Ed.* **2015**, *54*, 6814.

7. Halder, A.; Karak, S.; Addicoat, M.; Bera, S.; Chakraborty, A.; Shebeeb, H. K.; Pachfule, P.; Heine, T.; Banerjee, R. *Angew. Chem. Int. Ed.* **2018**, *57*, 5797.

8. (a) Desiraju, G. R. *Acc. Chem. Res.* **2002**, *35*, 565. (b) Desiraju, G. R.; Steiner, T. *The weak hydrogen bond in structural chemistry and biology*. Oxford University Press: Oxford, **1999**.

9. Chen, Z.; Wang, H. I.; Teyssandier, J.; Mali, K. S.; Dumschlaff, T.; Ivanov, I.; Zhang, W.; Ruffieux, P.; Fasel, R.; Räder, H. J.; Turchinovich, D.; De Feyter, S.; Feng, X.; Kläui, M.; Narita, A.; Bonn, M.; Müllen, K. J. *Am. Chem. Soc.* **2017**, *139*, 3635.

10. (a) Wang, L.; Feng, X.; Ren, L.; Piao, Q.; Zhong, J.; Wang, Y.; Li, H.; Chen, Y.; Wang, B. *J. Am. Chem. Soc.* **2015**, *137*, 4920. (b) Sheberla, D.; Bachman, J. C.; Elias, J. S.; Sun, C.-J.; Shao-Horn, Y.; Dincă, M. *Nat. Mater.* **2017**, *16*, 220.

# Synopsis TOC

